Diffusion of Ge below the Si(100) Surface: Theory and Experiment

Blas P. Uberuaga,[1,2] Michael Leskovar,[1,*] Arthur P. Smith,[2,†] Hannes Jónsson,[1,2,‡] and Marjorie Olmstead[1]

[1]*Department of Physics, Box 351560, University of Washington, Seattle, Washington 98195-1560*

[2]*Department of Chemistry, Box 351700, University of Washington, Seattle, Washington 98195-1700*

(Received 22 September 1999)

We have studied diffusion of Ge into subsurface layers of Si(100). Auger electron diffraction measurements show Ge in the fourth layer after submonolayer growth at temperatures as low as 500 °C. Density functional theory predictions of equilibrium Ge subsurface distributions are consistent with the measurements. We identify a surprisingly low energy pathway resulting from low interstitial formation energy in the third and fourth layers. Doping significantly affects the formation energy, suggesting that *n*-type doping may lead to sharper Si/Ge interfaces.

PACS numbers: 68.35.Fx, 68.35.Ct, 68.35.Dv, 68.35.Md

Interface abruptness in Si-Ge heterostructures has been the subject of intense research for many years [1]. Such heterostructures are of increasing interest for optoelectronic devices and quantum wells. Accurate modeling of these devices requires knowledge of the interface elemental profile. The lower surface energy and larger size of Ge relative to Si means that interdiffusion is thermodynamically favored when Si is deposited on Ge(100) [2]. In the reverse case, where Ge is deposited on Si(100), it has frequently been assumed that the interface is abrupt within 1–2 layers. Recently, evidence for Ge diffusion to the third [3–6] and fourth layer [7] has been reported, although other work found no significant interdiffusion at similar temperatures [8].

Diffusion of Ge in bulk Si has a large activation energy, on the order of 4–5 eV [9,10], and is negligible at the temperature of typical deposition experiments, about 500 °C. This high activation energy has been taken as an indication that Ge diffusion below the second layer of the Si(100) surface would be kinetically hindered, even if thermodynamically favored. Yet, several experimental measurements have indicated the presence of subsurface Ge [3–7]. The experimental results presented here suggest an activation barrier smaller than 2.5 eV for diffusion down to the fourth layer [11]. It has been suggested that the mechanism for subsurface diffusion must involve surface defects to facilitate transport [12].

In this Letter, we report experimental evidence for extensive interdiffusion during growth of Ge on Si(100), with Ge present throughout the top four layers after deposition of only 0.8 monolayer (ML) at 500 °C. The results are not strongly dependent on step structure (widely spaced, single-height steps vs closely spaced, double-height steps). We present results of theoretical calculations explaining these measurements. Density Functional Theory (DFT) calculations of relative site energies were carried out and used to predict the thermodynamic distribution of Ge atoms. Extensive calculations of diffusion paths and activation energies revealed a mechanism which could lead to near-equilibrium Ge distribution down to fourth layer without the presence of surface defects. Dopants are predicted to significantly affect the rate of Ge diffusion.

MgK_α-excited Auger and photoelectron diffraction (AED and PED) were used to determine the near-surface Ge distribution in Ge/Si(100) films. High kinetic energy PED/AED is a powerful tool for obtaining element-specific structure of the near-surface region [13]. Emission from Ge atoms occupying different sites may be distinguished by different angles of forward scattering by overlying atoms.

Figure 1 illustrates the dimerized Si(100) surface structure. The open structure and inhomogeneous stress distribution may affect Ge incorporation in subsurface sites. The tendency of the larger Ge atom to occupy tensile sites (labeled 3b, 4b) has been suggested as a mechanism for growth-induced ordering in $Si_{0.5}Ge_{0.5}$ alloys [14].

Si(100) wafers, both on axis and 4° toward [011], were cleaned with acetone and methanol, and outgassed overnight in ultrahigh vacuum (base pressure 2×10^{-10} torr) at 600 °C (resistive heating). The oxide was removed by annealing at high temperature (~1200 °C) until a sharp low-energy electron diffraction (LEED)

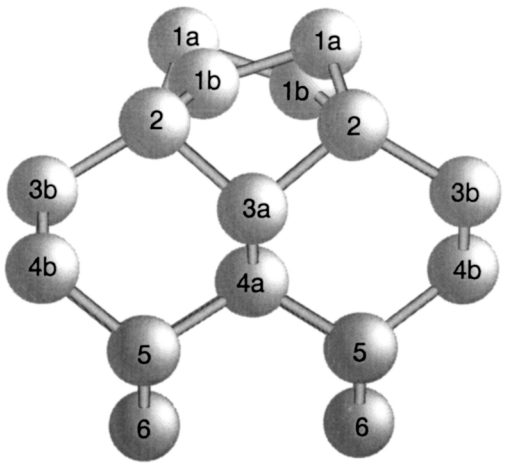

FIG. 1. Si(100)-$c4 \times 2$ surface structure. The reconstruction results in two inequivalent sites in layers 1, 3, and 4, but one site in layers 2, 5, and 6.

pattern was observed and no oxygen or carbon was detected by x-ray photoelectron spectroscopy. On-axis samples showed double domain $2 \times 1 + 1 \times 2$ LEED patterns. Off-axis samples showed single-domain 2×1 LEED, with spots split due to ordered, double-height steps [15]. Germanium was deposited by molecular beam epitaxy at 0.8 Å/min. Samples were annealed at 500 °C for 20 min immediately following deposition. Weak $2 \times n$ ($n = 8$–10) LEED spots, indicative of Ge dimer vacancy ordering [8], were observed after Ge deposition on on-axis samples. No faceting or other evidence of Ge islanding was observed. To prevent oxidation during data acquisition, samples were exposed to atomic hydrogen after cooling to room temperature (10^{-6} torr H_2 for 5 min, with sample facing a hot filament).

AED, PED, and LEED data were obtained for a matrix of Ge thickness (0.8 and 1.6 ML), substrate growth temperature (500 and 700 °C), and substrate step structure [widely separated, single-height steps (on axis) and closely spaced, double-height steps (4° miscut)] [16]. For PED/AED, electrons were detected by a hemispherical analyzer with an acceptance cone of ~4°. The angle between incident photons and emitted electrons, both in the horizontal plane, was fixed at 55°; the sample rotated around the vertical axis ($\theta = 0$ for normal emission) and the sample normal ($\phi = 0$ along [110]). Spectra were taken at each of 638 points evenly distributed (3.5° spacing) on a 90° partial hemisphere. Element-specific diffraction patterns for Si and Ge were obtained using intensities of Si $2p$ (PED) and Ge LMM (AED) emission, respectively. The presented data are normalized by the instrumental response; angles were aligned using the Si $2p$ emission.

In the absence of a kinetic pathway to subsurface sites, deposition of sub-ML Ge on Si(100) should result in Ge entirely in the top layer, with perhaps a small amount in layer 2 due to random burial or Si-Ge exchange. Such a distribution has been deduced from comparison of theoretical calculations with the coverage dependence of the $2 \times n$ reconstruction [8]. The predicted Ge photoelectron diffraction pattern for 0.8 ML deposition for such a distribution would be featureless except for a weak peak due to layer 2 Ge scattering from dimer atoms ($\theta \sim 60°, \phi \sim 13°, 77°$). Experimental results for on-axis wafers for 0.8 and 1.6 ML deposition at 500 and 700 °C are shown in Figs. 2(a)–2(c). The experimental results clearly show diffraction structure, indicating Ge buried to at least the fourth layer. Figure 2(d) shows the predicted AED pattern for our model described in detail below.

The bright spots in Fig. 2 indicate diffraction peaks. At these high kinetic energies (1140 eV), AED is dominated by forward scattering peaks surrounded by dark rings. The peak positions marked by circles in Fig. 2 are those predicted for Ge emission from the various sites indicated in Fig. 1 [labeled in Fig. 2(d)]. The single-scattering AED calculations used coordinates we calculated by DFT for H-terminated Si(100). The weak but observable layer 2

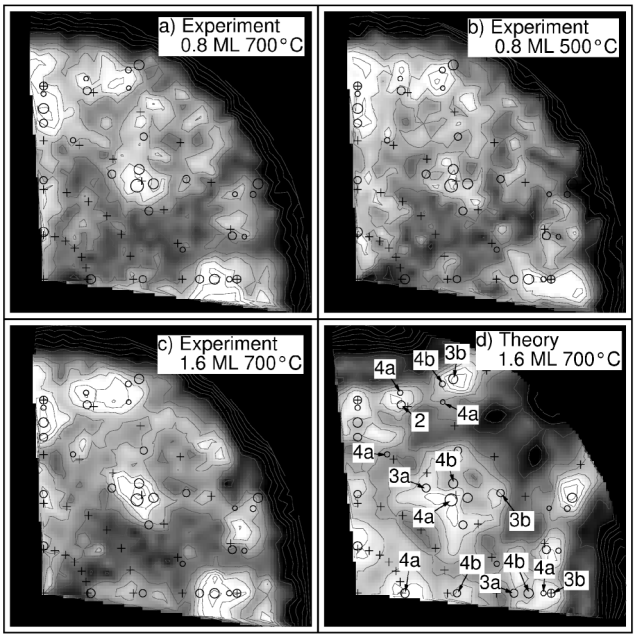

FIG. 2. Experimental (a)–(c) and theoretical (d) AED stereographic projections for Ge deposition on on-axis Si(100): (a) 0.8 ML Ge, $T_s = 700$ °C; (b) 0.8 ML, 500 °C; (c) 1.6 ML, 700 °C; (d) simulated AED for 1.6 ML, 700 °C based on occupations in Table I. Circles denote expected positions of peaks due to various emitters, labeled in (d), with the size indicating intensity. Plus signs are on a 15° grid. Contour lines are 4% of average emission intensity.

emission is in contrast to the absence of layer 2 Ge predicted for Si-Ge alloys using the Tersoff potential [17], but in agreement with our own *ab initio* calculations (see below). Ge occupation of layers 3 and 4 is clearly visible in the data, with larger occupation in the sites between dimer rows (3b, 4b) than beneath them (3a, 4a). For example, note the layer 4 peaks along $\phi = 0°$ and 90°, especially at 700 °C. Significant layer 4 (or deeper) occupation is indicated by the strong peak, present in all data sets, in the [110] direction ($\theta = \phi = 45°$). The [110] peak intensity increases by ~30% as the deposition temperature is increased from 500 °C [Eq. 2(b)] to 700 °C [Eq. 2(a)], and by another ~50% from 0.8 to 1.6 ML at 700 °C.

Experiments on off-axis samples (single-domain terraces separated by double-height steps) show similar AED results to the on-axis data of Fig. 2. The data are difficult to quantify due to uncertainties in the ratio of 2×1 to 1×2 domains after deposition. However, all peaks characteristic of Ge buried to the fourth layer are clearly present for off-axis wafers, in roughly the same ratios as for on-axis wafers. This indicates an incorporation mechanism based on terraces rather than steps.

The experimental measurements indicate significant subsurface occupation at both 500 and 700 °C, regardless of step structure. The dimer vacancy spacing for the on-axis samples is about the same as the step spacing for the off-axis samples, suggesting that neither greatly influence the results. Our AED patterns are also similar to those of Yeom *et al.* [7], who deposited Ge at room

temperature and annealed to 500 °C. They deduced a Ge distribution in the ratio 4:1:1:1 for the top four layers, but did not distinguish between *a* and *b* sites. The questions remain: (1) Why do Ge atoms get buried so deeply and (2) how are the kinetic barriers overcome? DFT calculations were carried out to answer these questions.

The DFT calculations were conducted with the VASP (Vienna *ab initio* simulation program) code [18], using ultrasoft pseudopotentials [19]. A plane wave basis set with an energy cutoff of 188 eV for the expansion of the wave function and the PW91 [20] exchange-correlation functional were used. In some cases, we quote results of calculations using the local density approximation (LDA) for comparison. Ge site energy calculations used a 64 atom cell with a vacuum spacing (the distance in the z direction between the periodically repeated slabs) of 11 Å and a $2 \times 2 \times 2$ k-point sampling mesh of the Monkhorst-Pack type [21] in the irreducible Brillouin zone. Migration pathway calculations used a 96 plus 1 atom cell, a vacuum spacing of 6 Å, and a $2 \times 2 \times 1$ k-point mesh. The nudged elastic band (NEB) method [22], implemented to run in parallel on a cluster of computers, was used to find the minimum energy paths (MEPs) for the transitions. About 20 metastable structures were found and 20 MEPs between them were calculated.

We first address the population of Ge in various sites of the Si surface. Letting n denote the probability of occupation of a site by a Ge atom, the free energy is [23]

$$F = n(E - \mu) - k_B T[n \ln(n) + (1 - n)\ln(1 - n)], \quad (1)$$

where E is the energy cost of substituting a Ge atom for a Si atom at the site, μ the chemical potential of Ge, T the absolute temperature, and k_B the Boltzmann constant. Minimizing this free energy with respect to n leads to

$$n = (E, T, \mu) = \frac{e^{(\mu - E)/(k_B T)}}{1 + e^{(\mu - E)/(k_B T)}}, \quad (2)$$

the Fermi-Dirac distribution. We adjust μ so the total amount of Ge in the model is equal to the amount deposited during the experiment. One should include effects of vibrational and configurational entropy when calculating the fractional occupation of Ge. We find that their inclusion (as done in detailed Monte Carlo simulations [17]) changes the occupation numbers by less than 15%, and is thus neglected here. We applied this model using substitutional energy E found with DFT. Table I gives the calculated energies and resultant occupation numbers for the various sites after deposition of 0.8 ML at 500 and 700 °C and 1.6 ML at 700 °C.

These calculations show that, even for 0.8 ML deposition at 500 °C, an appreciable amount of Ge is predicted thermodynamically to be found in the third and fourth layers. The amount increases with temperature and deposition amount. For 1.6 ML of deposition at 700 °C, almost one third of both the 3b and 4b sites are predicted to contain Ge. The subsurface sites underneath the trough are predicted to have the largest occupations, in agreement with earlier calculations using an empirical potential [24]. However, unlike that study, we find the occupation of layer 2 to be nearly the same as these tensile sites, which agrees with the experimental results. The tensile strain on these sites due to the surface reconstruction is more accommodating for the larger Ge atom. We have simulated the AED spectra based on these occupation numbers and find that the results are in good qualitative agreement with the experiment, as shown in Fig. 2. The stronger layer 4 signals in the experiment than in the calculated pattern could arise either from additional layer 4 occupation or from approximations in the AED simulations (single scattering; all Si atoms).

Experiments have shown that Ge diffuses in bulk Si by both substitutional-interstitial exchange and a vacancy mechanism, with comparable contribution with each [25]. We focus here on the former mechanism. The exchange process where a Si interstitial displaces a Ge atom from a lattice site in the bulk, $Si_I + Ge_L \rightarrow Si_L + Ge_I$, has a small activation barrier. Our DFT calculations give a barrier of 0.3 eV and the exchange is downhill by ~0.1 eV. This process, in which Ge diffusion is assisted by a Si interstitial, is of lower energy than Ge directly diffusing through the crystal. *The dominant part of the activation energy for Ge diffusion is the formation energy of the Si interstitial.* This has been estimated to be 3.3 eV using LDA [26] and our PW91 calculations give 3.7 eV. This gives a total activation energy for bulk Ge diffusion of 4.0 eV within DFT. The central question is the following: *What is the formation energy of Si interstitials near the surface?* Since Ge displaces surface Si upon deposition [6], both Si and Ge adatoms are present during growth; we calculate the interstitial energy with respect to the Si adatom. We find the formation energy of Si self-interstitials in the surface region to be significantly lower than in the bulk. Figure 3 shows the formation energy of interstitials as well

TABLE I. Energy cost of substituting a Ge atom for Si in various sites near the Si surface relative to 1a and calculated fractional occupations. The site labels are explained in Fig. 1. Results of LDA and PW91 DFT calculations as well as an empirical interaction potential [29] are given. The fractional occupations are based on the PW91 values and Eq. (2), and correspond to experimental conditions of 0.8 ML Ge coverage at substrate temperatures of 500 and 700 °C and 1.6 ML at 700 °C.

	Energy (eV)			Fractional occupation 0.8 ML		1.6 ML
Layer	LDA	PW91	Tersoff	500 °C	700 °C	700 °C
1a	0.000	0.000	0.000	0.904	0.831	0.965
1b	0.134	0.149	···	0.495	0.449	0.820
2	0.314	0.363	0.230	0.037	0.058	0.257
3a	0.361	0.415	0.136	0.017	0.032	0.156
3b	0.292	0.344	0.123	0.049	0.072	0.303
4a	0.344	0.419	0.174	0.016	0.031	0.150
4b	0.291	0.348	0.107	0.046	0.069	0.293

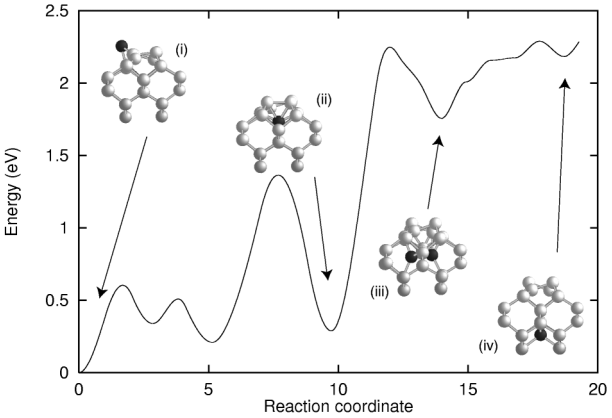

FIG. 3. Minimum energy path calculated by DFT for the diffusion of a Si adatom to subsurface interstitial sites down to the fifth layer. The activation energy to bring an adatom to layer 4 is 2.2 eV. Stable structures include: (i) the adatom, (ii) a dumbbell in layer 3, (iii) a dumbbell in layer 4, and (iv) a tetrahedral interstitial in layer 5.

as a possible pathway for a Si adatom to reach the fifth layer. Even in the fifth layer, the nature of the interstitial is different than in bulk. The optimal configuration is a tetrahedral interstitial [Fig. 3(iv)] rather than a dumbbell [Fig. 3(iii)] [27]. The low energy of interstitials near the Si(100) surface is consistent with calculations of Tersoff for C diffusion in Si using his empirical interaction potential [28].

The migration path (Fig. 3) involves the hop of an adatom (i) on top of a dimer row, and then displacement of the adatom down between two surface dimers to a dumbbell interstitial geometry perpendicular to the surface dimers (ii) where it shares a third layer site with a lattice atom. One of these atoms pushes an atom out of the fourth layer, forming a dumbbell parallel to the surface dimers with an energy of 1.8 eV relative to the adatom (iii). One of these atoms can jump further down into the fifth layer, forming a tetrahedrally coordinated interstitial (iv). This configuration is about 2.2 eV above the adatom in energy. The barrier for formation of the interstitial in the fourth layer (iii) is 2.2 eV with respect to the Si adatom. The overall barrier for Ge diffusion down to the fourth layer is estimated to be 1.8 eV + 0.3 eV = 2.1 eV (after adding 0.3 eV for the Si/Ge exchange) [29], on the order of the upper bound set by the experimental conditions [11].

Finally, we have seen a significant effect in these calculations of the charge state of the system. The stability of the fifth layer interstitial compared to the adatom goes from 2.6 eV at a charge of -2 to 1.6 eV at $+2$. The insertion of boron with the accompanying loss of an electron has a similar effect, stabilizing the interstitial by 0.5 eV compared to pure Si. This suggests that the Ge/Si interface may be sharper for n-type than for p-type substrates.

We would like to thank J. Tersoff, E. Kaxiras, and M. Lagally for helpful discussions, and S. Meng for assistance with AED modeling and data acquisition. This work was funded by NSF Grant No. CHE-9710995, the Japanese New Energy Development Organization, and the University of Washington Royalty Research Fund. Part of the calculations presented here were carried out on a cluster of PCs donated by Intel Co.

*Present address: The Boeing Company, P.O. Box 3707, M/C 42-85, Seattle, WA 98124.
†Present address: American Physical Society, 1 Research Road, Ridge, NY 11961.
‡Electronic address: hannes@u.washington.edu

[1] F. Schaffler, Semicond. Sci. Technol. **12**, 1515 (1997).
[2] D. S. Lin, T. Miller, and T. C. Chiang, Phys. Rev. B **45**, 11 415 (1992).
[3] H. Oyanagi *et al.*, Jpn. J. Appl. Phys. **33**, 3545 (1994).
[4] A. Ikeda *et al.*, Surf. Sci. **385**, 200 (1997).
[5] R. Gunnella *et al.*, Phys. Rev. B **54**, 8882 (1996).
[6] L. Patthey *et al.*, Phys. Rev. Lett. **75**, 2538 (1995).
[7] H. W. Yeom *et al.*, Surf. Sci. **381**, L534 (1997).
[8] F. Liu and M. G. Lagally, Phys. Rev. Lett. **76**, 3156 (1996).
[9] P. Dorner *et al.*, Philos. Mag. **49**, 557 (1984).
[10] G. Hettich, H. Mehrer, and K. Maier, in *Defects and Radiation Effects in Semiconductors*, edited by J. H. Albany, Institute of Physics Conference Series (Institute of Physics, London, 1979), p. 500.
[11] Assuming the onset of the diffusion mechanism corresponds to the experimental conditions of the present study, ca. 100 sec at 500 °C, and a standard prefactor for surface diffusion, 10^{-13} sec^{-1}, an activation energy of 2.3 eV is obtained within harmonic transition state theory.
[12] X. Y. Zhu and Y. H. Lee, Phys. Rev. B **59**, 9764 (1999).
[13] W. F. Egelhoff, CRC Crit. Rev. Solid State Sci. **16**, 213 (1990).
[14] F. K. LeGoues *et al.*, Phys. Rev. Lett. **64**, 2038 (1990).
[15] R. D. Bringans *et al.*, Phys. Rev. B **34**, 7447 (1986).
[16] M. A. Leskovar, Ph.D. dissertation, University of Wshington, 1998.
[17] P. C. Kelires and J. Tersoff, Phys. Rev. Lett. **63**, 1164 (1989).
[18] G. Kresse and J. Hafner, Phys. Rev. B **47**, 558 (1993); **49**, 14 251 (1994); G. Kresse and J. Furthmüller, Comput. Mater. Sci. **6**, 16 (1996); Phys. Rev. B **54**, 11 169 (1996).
[19] D. Vanderbilt, Phys. Rev. B **41**, 7892 (1990).
[20] J. P. Perdew, in *Electronic Structure of Solids*, edited by P. Ziesche and H. Eschrig (Akademie Verlag, Berlin, 1991).
[21] H. J. Monkhorst and J. D. Pack, Phys. Rev. B **13**, 5188 (1976).
[22] H. Jónsson, G. Mills, and K. W. Jacobsen, in *Classical and Quantum Dynamics in Condensed Phase Simulations*, edited by B. J. Berne *et al. (*World Scientific, Singapore, 1998), Ch. 16.
[23] D. Chandler, *Introduction to Modern Statistical Mechanics* (Oxford University Press, New York, 1987).
[24] J. Tersoff, Phys. Rev. B **39**, 5566 (1989).
[25] P. Fahey, S. S. Iyer, and G. J. Scilla, Appl. Phys. Lett. **54**, 843 (1989).
[26] P. E. Blöchl *et al.*, Phys. Rev. Lett. **70**, 2435 (1993).
[27] W.-K. Leung *et al.*, Phys. Rev. Lett. **83**, 2351 (1999).
[28] J. Tersoff, Phys. Rev. Lett. **74**, 5080 (1995).
[29] The barrier is 2.7 eV with respect to a kink atom, which is 0.6 eV lower in energy than an adatom.